Benefits of the Coupled Inductors Combined Cuk-SEPIC (CI-CCS) Converter

K S Nathan, **S S Ghosh***, **P R Tripathi***, **Y P Siwakoti**†, **T J Flack***, **X Li***, **T Long****

**Department of Engineering, University of Cambridge, United Kingdom*

ksn26@cam.ac.uk, ssg39@cam.ac.uk, prt36@cam.ac.uk, tjf1000@cam.ac.uk, xl418@cam.ac.uk, tl322@cam.ac.uk

†*Faculty of Engineering and IT, University of Technology Sydney, Australia, Yam.Siwakoti@uts.edu.au*

Keywords: CI-CCS converter, Cuk converter, SEPIC converter, coupled inductors, bipolar DC-DC converter

Abstract

An enhanced DC-DC converter is proposed in this paper, based on the combination of the Cuk and SEPIC converters. This converter uses a single switching node which is common to both Cuk and SEPIC energy transfer stages. The converter uses only one switch, yet provides dual outputs in the form of a bipolar DC bus with a common ground. Since the switch is grounded, a simple, non-isolated gate driver may be used. The proposed converter uses integrated magnetics cores to couple the input and output inductors, which significantly reduces the input current ripple. The new converter is referred to as the Coupled Inductors Combined Cuk-SEPIC (CI-CCS) converter.

1 Introduction

1.1 The Combined Cuk-SEPIC (CCS) Converter

There are several examples, including solar photovoltaics, DC microgrids, electric vehicle chargers, and drives, where a high step-up voltage conversion ratio, regulation of a widely-varying source, or a bipolar DC output, is needed. The combined Cuk-SEPIC (CCS) converter, shown in Figure 1, is an emerging DC-DC converter topology that is well-suited for these applications and has hence been investigated recently [1–5]. It uses a single switching node, which is common to both Cuk and SEPIC energy transfer stages, to provide matching ground-referenced positive and negative outputs. Alternatively, it can be used as a non-ground-reference output with twice the output voltage when loads are connected between the positive and negative terminals.

Compared with conventional DC-DC converters, the CCS converter can provide large step-up, as well as step-down voltage conversion ratios. The converter has an output/input voltage ratio of $^{2D}/_{(1-D)}$ (when considering the bipolar bus as a single output), compared with $^{1}/_{(1-D)}$ for regular step-up converters, and $^{D}/_{(1-D)}$ for regular step-up/down converters. Figure 2 shows the gain provided by these different converter types for a range of duty cycles. It can be seen that for duty ratios greater than 1/2, the CCS converter provides a higher step-up ratio than typical step-up converters. For duty ratios below 1/3, the converter operates in step-down mode.

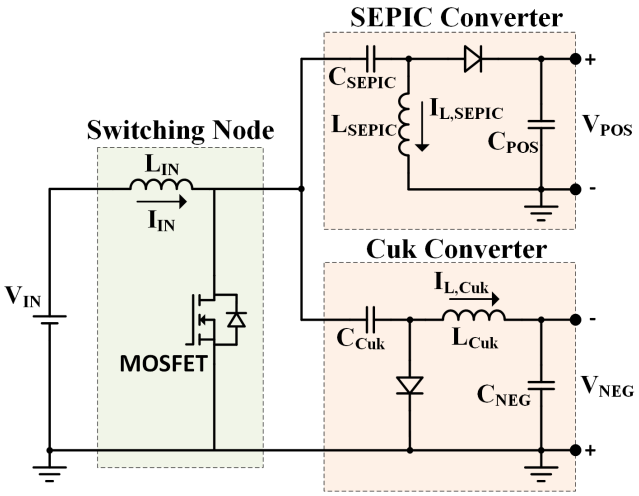

Figure 1: Combined Cuk-SEPIC (CCS) converter topology.

The distinct output/input voltage ratio allows regulation of larger input voltage variations with the same duty cycle range, or alternatively allows the converter to handle the same input voltage variation with a narrower duty cycle range, allowing for smaller inductors to be used. If a bipolar output is desired, then this converter provides both a positive and negative voltage equal to that of regular step-up/down converters.

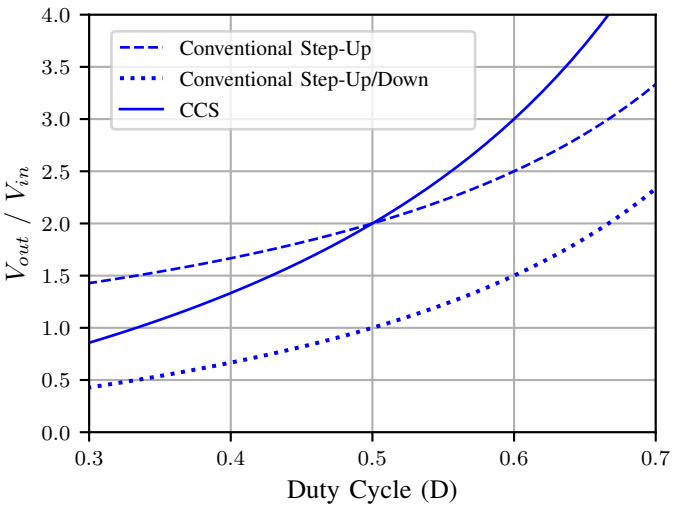

Figure 2: Voltage gain ratios for conventional step-up, step-up/down, and the CCS Converter.

1.2 Inductor Magnetic Coupling

The benefits of inductor coupling in Cuk converters and SEPIC converters has been described in the literature [5, 6]. Despite recent interest in the CCS converter however, research is yet to be conducted into the benefits of coupling its input and output inductors.

In this paper, the impact of coupling between L_{in}, L_{SEPIC}, and L_{Cuk}, as shown in Figure 1, is investigated. This converter is henceforth referred to as the Coupled Inductors Combined Cuk-SEPIC (CI-CCS) converter. Analysis shows that performance benefits can be realised if L_{SEPIC} and L_{Cuk} are independently coupled with L_{in}, but they should remain uncoupled from each other (essentially combining the coupled inductor parts of individual Cuk and SEPIC converters, with the unified input switching node of the CCS converter). This use of integrated magnetics means that the converter contains two distinct magnetic structures. A multi-variable optimisation has been conducted to determine the optimum coupling levels in Section 2, followed by simulation and experimental results in Sections 3 and 4 respectively. The results demonstrate that this coupling can significantly reduce the input current ripple, which allows the overall inductance – and hence volume and weight – to be reduced.

2 Converter Design and Magnetics Optimisation

A CCS converter was initially designed with no magnetic coupling between any of the inductors (as shown in Figure 1), to meet the specifications given in Table 1 (the input voltage range corresponds to a duty cycle of 0.5 ± 10%). It should be noted that the input current ripple (given as a percentage of average input current) specification is quite high, which allows the benefits of inductor coupling to be highlighted.

Nominal input voltage	360V
Input voltage range	294V to 440V
Target output voltage	± 360V
Rated output power	4 kW
Switching frequency	100 kHz
Input current ripple	40% peak-peak (at rated power)
Output voltage ripple	2% peak-peak (at rated power)

Table 1: Converter design specifications.

This design process resulted in the component values listed in Table 2.

C_{SEPIC}	1.19 µF
C_{Cuk}	0.47 µF
C_{POS}	4.68 µF
C_{NEG}	0.31 µF

L_{in}	546 µH
L_{SEPIC}	886 µH
L_{Cuk}	896 µH

Table 2: Converter component values.

This input inductance was then split into two inductors (L_{in1} in series with L_{in2}), and a multi-variable optimisation was conducted where the variables being tested were:

- Ratio of the split of L_{in1} and L_{in2}
- Coupling factor between L_{in1} and L_{Cuk} (k_1)
- Coupling factor between L_{in2} and L_{SEPIC} (k_2)
- Coupling factor between L_{SEPIC} and L_{Cuk} (k_3)

The optimisation process revealed that magnetic coupling between the output inductors (i.e. a non-zero value of k_3) had a detrimental impact on performance. It was also clear that no benefits were associated with having an unequal split of L_{in1} and L_{in2}, nor were there any advantages to distinct values of k_1 and k_2. Thus, it was possible to apply the constraints given in Equations (1), (2), and (3) to simplify the optimisation.

$$L_{in1} = L_{in2} = 0.5 \times L_{in} \quad (1)$$

$$k_1 = k_2 (= k) \quad (2)$$

$$k_3 = 0 \quad (3)$$

The results of this optimisation can be seen in Figure 3, which shows the sensitivity of the input current ripple against the coupling factor (L_{in} - L_{Cuk} and L_{in} - L_{SEPIC}) at rated power. The three lines show the input current ripple (as a percentage of average input current) at the nominal input voltage (360V), as well as at the limits of the input voltage range (294V and 440V). It is observed that the minimum ripple occurs at the same coupling factor (k = 0.89), independent of input voltage and voltage conversion ratio.

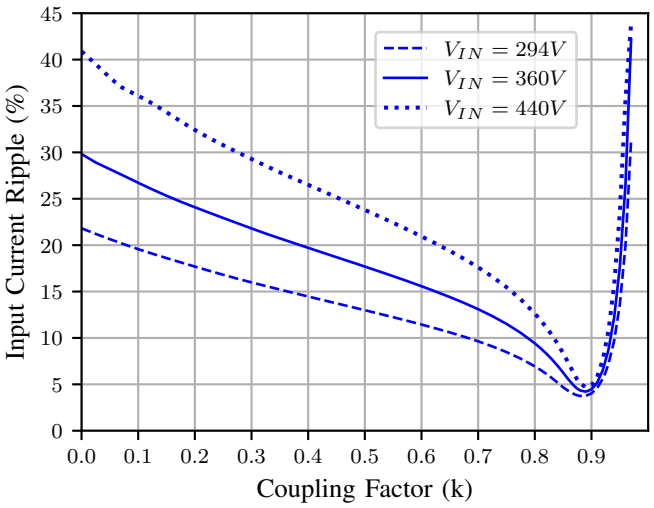

Figure 3: Input current ripple vs. coupling factor at rated power for the limit and nominal input voltages.

This result shows a significant decrease in input current ripple of more than 80% for all three input voltages, and forms the basis of the simulations and experimental work.

3 Simulation Results

The CCS converter has been simulated successfully using the Saber simulation package, in two key scenarios:

- Standard control scenario: no coupling between input, Cuk, and SEPIC inductors.
- Optimal scenario for input current ripple reduction: coupling factor of 0.89 between L_{in} - L_{Cuk} and L_{in} - L_{SEPIC}, and no coupling between L_{SEPIC} - L_{Cuk}.

For both of these scenarios, the converter was simulated at nominal input voltage (360V) as well as the limit input voltages (294V and 440V) by adjusting the duty cycle accordingly. The most relevant waveforms of these simulations are shown in Figure 4, which relates to the nominal input voltage condition. The key observation is the significant decrease in the input current ripple in the coupled inductors scenario, without negatively impacting any other component current or voltage waveforms.

The average input current remains the same regardless of coupling factor, however the ripple component is significantly reduced when a 0.89 coupling factor between input and output inductors is used. The input current ripple (peak-to-peak) as a percentage of average input current is shown in Table 3. These results demonstrate that a 0.89 coupling factor reduces input current ripple by 82% to 88% compared with the no coupling scenario.

Coupling	Input current ripple (percentage of average)		
	V_{in} = 294V	V_{in} = 360V	V_{in} = 440V
None (k = 0)	21.8%	29.7%	40.0%
Optimal (k = 0.89)	3.8%	4.2%	4.7%

Table 3: Input current ripple for no coupling and a coupling factor of 0.89, at nominal and limit input voltages.

The peak-to-peak output voltage ripple is calculated to be 1.8% for the positive DC output and 2% for the negative DC output, fulfilling the design requirements. These values remain largely constant over variations in both input voltage and coupling factor.

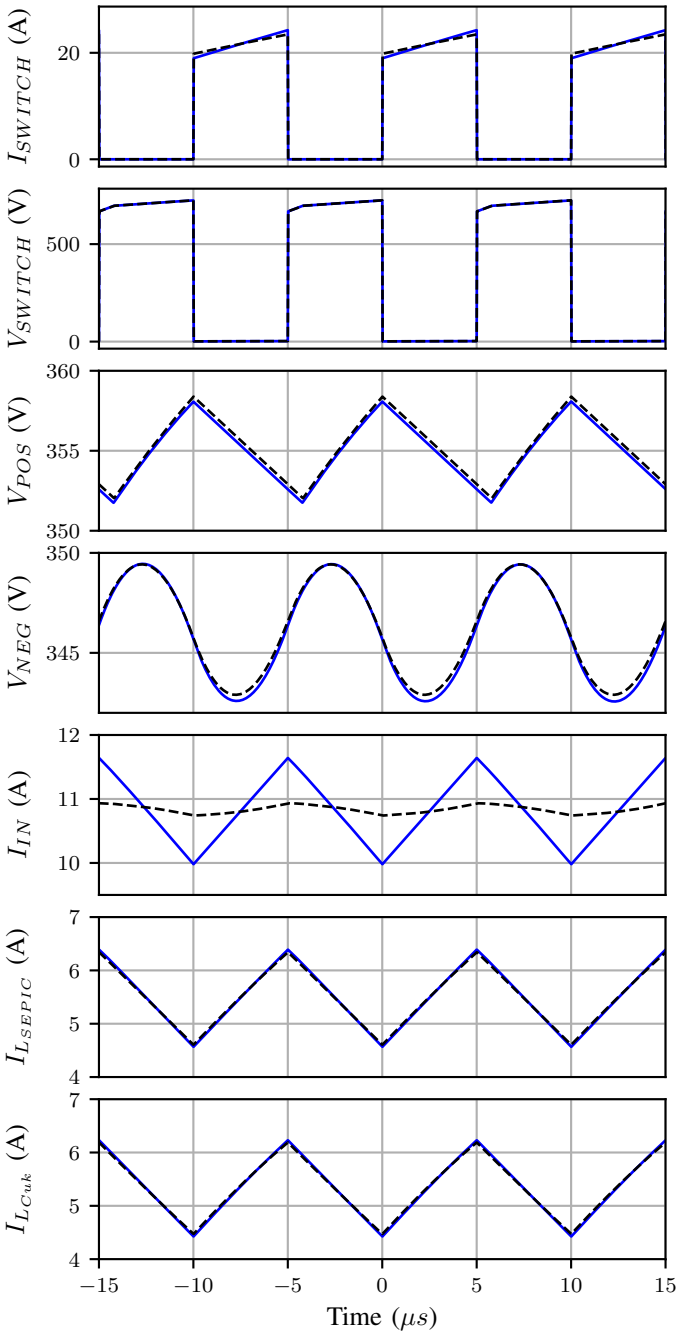

Figure 4: MOSFET current, MOSFET voltage (V_{DS}), V_{POS}, V_{NEG}, I_{IN}, $I_{L_{SEPIC}}$, $I_{L_{Cuk}}$ (with V_{IN} = 360V; no coupling - blue solid line, optimal coupling - black dotted line).

4 Experimental Validation

4.1 Testbed Design

An experimental prototype was built to provide a validation of the results obtained through the simulation studies and optimisations.

In the literature, an IGBT has been widely used as the CCS converter's switching device [2]. This limits the switching frequency, and hence power density, for high frequency power converter designs. Considering these aspects in designing a compact converter, a silicon carbide (SiC) MOSFET is implemented here to achieve higher volumetric and gravimetric power density and efficiency.

Film capacitors were also chosen over electrolytic capacitors due to their high voltage rating, higher RMS and peak current handling capabilities, as well as their better reliability. The primary benefit of electrolytic capacitors is a higher capacitance, however that is not a requirement for this converter.

A list of the components used in the experimental prototype

is:

- Cree Wolfspeed C3M0065100K SiC MOSFET
- STMicroelectronics STPSC20H12 SiC Schottky diodes
- Kemet R75MI33304030J (0.33 µF, 400V) capacitor
- Vishay MKP1848550704K2 (5 µF, 700V) capacitor
- Vishay MKP1840447104M (0.47 µF, 1kV) capacitor
- Kemet R71VN41504030K (1.5 µF, 520V) capacitor
- Texas Instruments UCC27531DBVT SiC MOSFET gate driver
- Texas Instruments TMS320F28379D microcontroller
- TE Connectivity TE1000B120RJ (120 Ω, 1 kW) load resistors
- Custom-made inductors (described in Section 4.2).

A photo of the developed prototype is shown in Figure 5 and the entire experimental testbed is shown in Figure 6. The PCB contains the SiC MOSFET, gate drive circuitry, SiC diodes, capacitors, and connectors (for the inductors, voltage source, and loads). The inductors are kept separate from the board to allow different coupling levels to be easily tested.

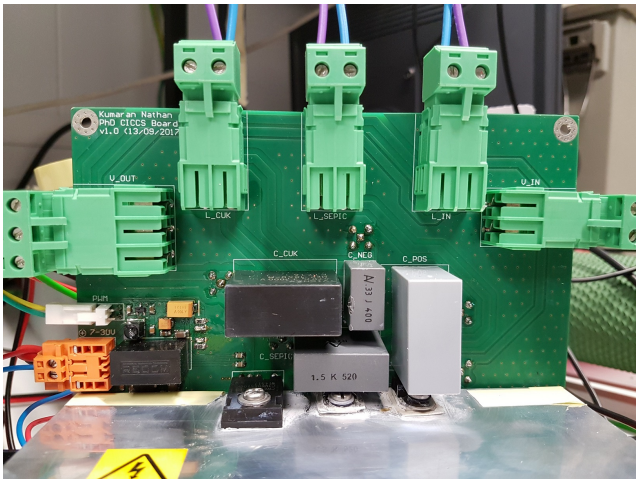

Figure 5: CI-CCS converter prototype.

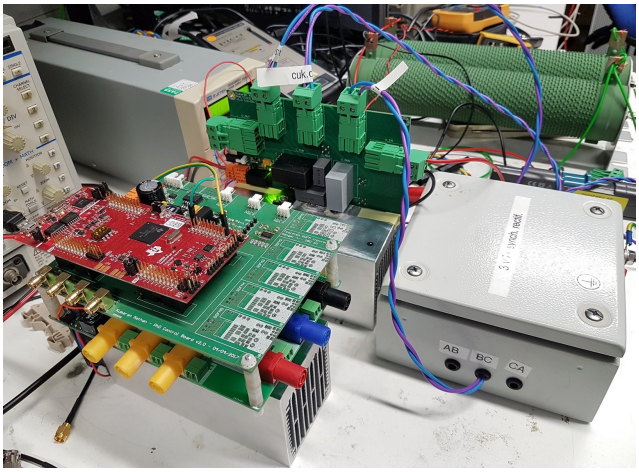

Figure 6: Experimental testbed.

4.2 Design and Construction of the Coupled Inductors

The choice of magnetic material for the inductor core is extremely important due to the high switching frequency and DC bias. Some important factors to consider when selecting the core material are the saturation point, permeability, and core losses.

It was not desirable to use an air core inductor due to the low permeability of air, which would ultimately result in an impractical number of turns being required. Iron powder cores were also eliminated as an option due to the requirement of switching at 100 kHz. Next, nanocrystalline ribbon cores were eliminated due to the DC bias present in the inductor currents due to a very large permeability (up to 500,000) and high propensity to saturate under DC bias conditions [7]. Thus, the remaining options were ferrite cores and nanocrystalline powder cores.

Nanaocrystalline powder cores have an advantage over ferrite cores for DC line reactor applications due to their homogeneous low permeability. Nanocrystalline powder cores are formed with distributed micro air gaps to control the permeability (normally from 60 to 120) and avoid saturation of flux density caused by the large magnetic forces created from the DC currents. Due to ferrite's naturally high permeability (normally several thousand), additional air gaps must be inserted between ferrite core pieces when making the inductor in order to achieve low permeability. This can lead to more complex and difficult designs and inconsistent performance. Additionally, the saturation point of nanocrystalline-based materials is more than double that of ferrite, which further supports the use of nanocrystalline powder cores in DC line reactors [8].

This paper aims to produce an experimental prototype to demonstrate the proof of concept (i.e. that substantial ripple reduction can be achieved). Thus, cost and ease of construction were prioritised over a custom core design (which would become more important for a commercial product). A solution was developed that used standard inductor core dimensions (H57), that have tightly coupled windings, in series with uncoupled inductors on separate cores. An illustration of this is shown in Figure 7.

The total and mutual inductances of the coupled inductors in Figure 7a are:

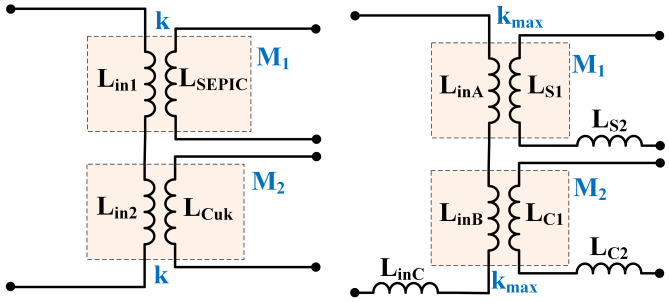

(a) Specialised Coupled Inductors.

(b) Simple Equivalent Coupled Inductors.

Figure 7: Specialised vs. simple equivalent coupled inductors.

$$L_{in} = L_{in1} + L_{in2} \tag{4}$$
$$L_{SEPIC} = L_{SEPIC} \tag{5}$$
$$L_{Cuk} = L_{Cuk} \tag{6}$$
$$M_1 = k\sqrt{L_{in1} \times L_{SEPIC}} \tag{7}$$
$$M_2 = k\sqrt{L_{in2} \times L_{Cuk}} \tag{8}$$

Similarly, the total and mutual inductances of the tightly coupled inductors in Figure 7b are:

$$L_{in} = L_{inA} + L_{inB} + L_{inC} \tag{9}$$
$$L_{SEPIC} = L_{S1} + L_{s2} \tag{10}$$
$$L_{Cuk} = L_{C1} + L_{C2} \tag{11}$$
$$M_1 = k_{max}\sqrt{L_{inA} \times L_{S1}} \tag{12}$$
$$M_2 = k_{max}\sqrt{L_{inB} \times L_{C1}} \tag{13}$$

To eliminate the need for L_{inC}, let $L_{inA} = L_{inB} = 0.5 \times L_{in}$. If two coils tightly wound on the same toroidal core have a coupling factor of k_{max}, then L_{S1} and L_{C1} can be calculated as shown in Equations (14) and (15), where M_1 and M_2 are obtained from the desired values given in Equations (7) and (8).

$$L_{S1} = \frac{\left(\frac{M_1}{k_{max}}\right)^2}{0.5 \times L_{in}} \tag{14}$$
$$L_{C1} = \frac{2\left(\frac{M_2}{k_{max}}\right)^2}{0.5 \times L_{in}} \tag{15}$$

It is then easy to calculate L_{S2} and L_{C2} as per Equations (16) and (17).

$$L_{S2} = L_{SEPIC} - L_{S1} \tag{16}$$
$$L_{C2} = L_{Cuk} - L_{C1} \tag{17}$$

This means that the overall mutual and self inductance (and hence performance) are identical to what would be obtained with a specialised inductor design. The main trade-off however, is the increased number of cores (4 compared with 2).

Both the uncoupled and coupled inductors used in the experimental tested are shown in Figure 8.

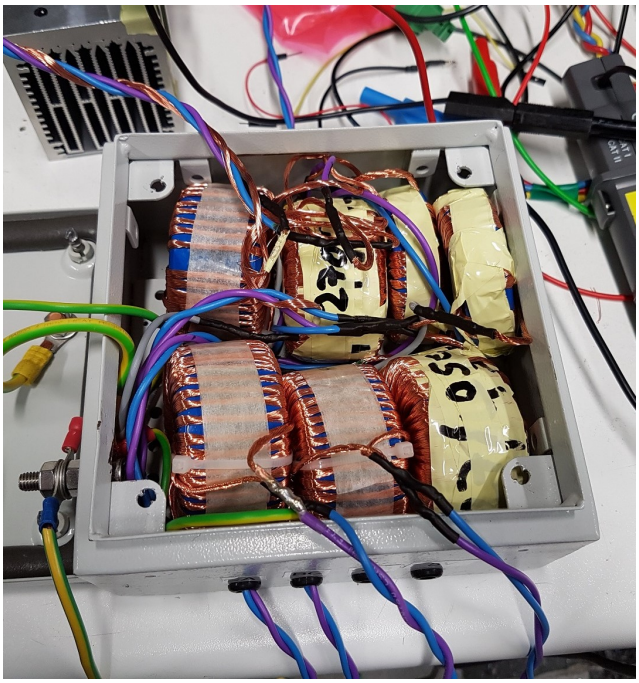

Figure 8: Coupled and uncoupled inductors.

4.3 Results

The results presented in this section demonstrate the operation and performance of the converter using both uncoupled and coupled inductors. The experimental results are shown in Figure 9, showing the large reduction in input current ripple.

The experimental results have ringing at 1.8 MHz due to parasitics present (primarily the inter-turn capacitance of the inductor windings, but also stray inductance in the current paths for the MOSFET, diodes, and capacitors). This ringing could be substantially reduced with improved inductor and PCB design, however that is not the primary focus of this paper. For the sake of clarity in demonstrating the relevant results, post-processing has been performed with a zero-phase low-pass filter to reduce this ringing. The filtering does not affect the comparison presented as the ringing is equal for both the uncoupled and coupled inductors.

When all inductors are left uncoupled, the peak-to-peak input current ripple is 30.2%. When the integrated magnetics are

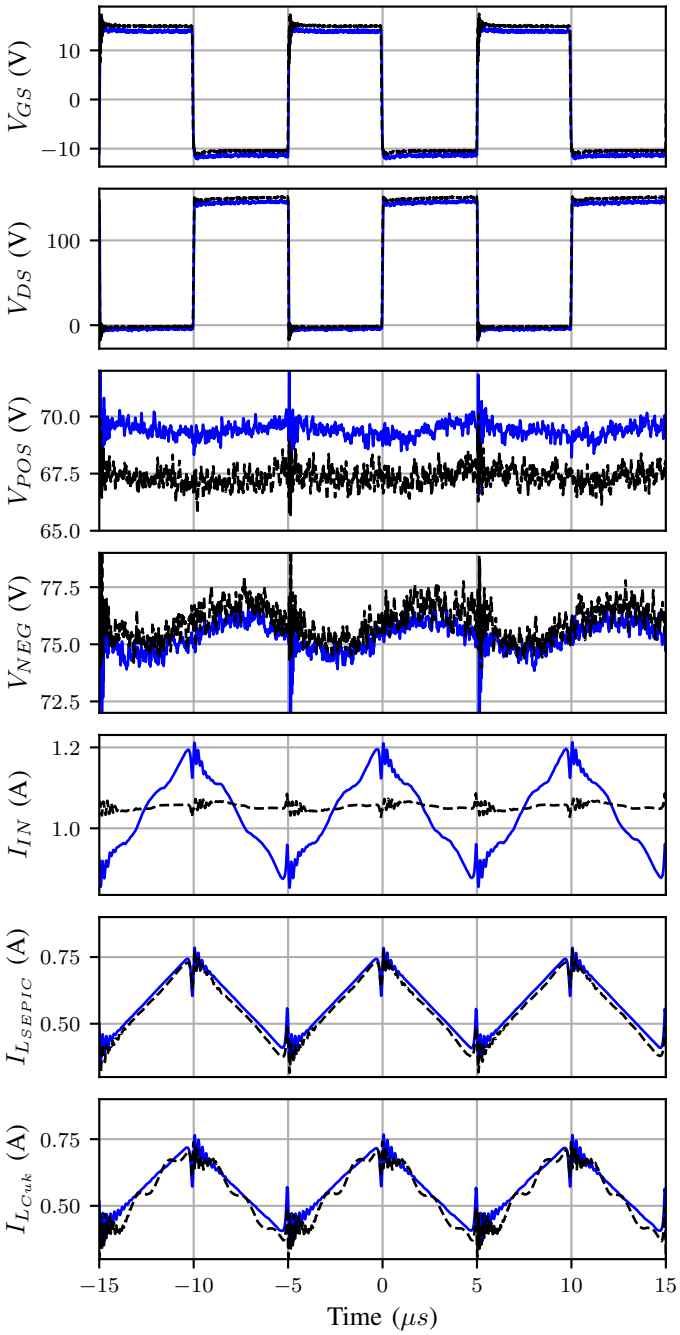

Figure 9: Switch signal, MOSFET voltage (V_{DS}), V_{POS}, V_{NEG}, I_{IN}, $I_{L_{SEPIC}}$, $I_{L_{Cuk}}$ (with V_{IN} = 80V; no coupling - blue solid line, optimal coupling - black dotted line).

introduced, the peak-to-peak current ripple drops to just 2.0%, representing a reduction of more than 93%.

It can also be seen that there is a very minor imbalance between the positive and negative output voltages due to component non-idealities impacting each converter differently. The peak-to-peak output voltage ripple is calculated to be 1.2% for the positive DC output and 2.3% for the negative DC output. These values remain largely constant over variations in both input voltage and coupling factor, and agree closely with the simulation results.

5 Conclusion

Combining the input stages of the Cuk and SEPIC converters allows a bipolar DC output to be generated from a unipolar input, using only a single switch. This emerging converter topology shows many advantages and much potential. The converter can also be used as a single, large, non-ground-referenced DC bus, with the load connected between the positive and negative outputs.

In this paper, the benefits that can be derived by magnetically coupling the converter's input and output inductors are investigated for the first time. SiC power devices and nanocrystalline powder cores are also used, in place of IGBTs and ferrite cores. This has enabled much higher switching frequencies, and together with the coupled inductors, minimal input current ripple has been realised. Results have been obtained, both in simulations and experimentally, which show that input current ripple reductions of 80-93% are possible with the same inductor values and appropriate coupling factor selection.

Acknowledgements

The authors would like to express their appreciation for the following funding sources: The General Sir John Monash Foundation, the Cambridge Trust (in partnership with Cambridge Australia Scholarships), and the Isaac Newton Trust.

References

[1] A. Anand and B. Singh, "Power Factor Correction in Cuk-SEPIC Based Dual Output Converter fed SRM Drive," *IEEE Transactions on Industrial Electronics*, pp. 1–1, 2017.

[2] M. B. Ferrera, S. P. Litran, E. Duran Aranda, and J. M. Andujar Marquez, "A Converter for Bipolar DC Link Based on SEPIC-Cuk Combination," *IEEE Transactions on Power Electronics*, vol. 30, no. 12, pp. 6483–6487, dec 2015.

[3] M. B. Ferrera, S. P. Litran, E. Duran, and J. M. Andujar, "A SEPIC-Cuk converter combination for bipolar DC microgrid applications," in *2015 IEEE International Conference on Industrial Technology (ICIT)*. IEEE, mar 2015, pp. 884–889.

[4] B.-R. Lin, K.-L. Shih, J.-J. Chen, and H.-K. Chiang, "Implementation of a zero voltage switching Sepic-Cuk converter," in *2008 3rd IEEE Conference on Industrial Electronics and Applications*. IEEE, jun 2008, pp. 394–399.

[5] N. Jayaram and D. Maksimovic, "Power factor correctors based on coupled-inductor Sepic and Cuk converters with nonlinear-carrier control," in *APEC '98 Thirteenth Annual Applied Power Electronics Conference and Exposition*, vol. 1. IEEE, pp. 468–474.

[6] L. Mohammadian and E. Babaei, "Investigating the effect of inductor coupling on intrinsic stability of Cuk converter," in *IECON Proceedings (Industrial Electronics Conference)*. IEEE, oct 2016, pp. 1359–1364.

[7] X. Wang, Z. Lu, C. Lu, and D. Li, "Fe-based nanocrystalline powder cores with ultra-low core loss," *Journal of Magnetism and Magnetic Materials*, vol. 347, pp. 1–3, dec 2013.

[8] G. T. Nikolov and V. C. Valchev, "Nanocrystalline magnetic materials versus ferrites in power electronics," *Procedia Earth and Planetary Science*, vol. 1, no. 1, pp. 1357–1361, sep 2009.